Designing Highly Stable Poly(sarcosine)-based Telodendrimer Micelles with High Drug Content Exemplified with Fulvestrant

Qing Yu[1], Richard M. England[1]*, Anders Gunnarsson[2], Robert Luxenhofer[4,5], Kevin Treacher[3], Marianne B. Ashford[1]

[1]Advanced Drug Delivery, Pharmaceutical Sciences, R&D, AstraZeneca, Macclesfield, SK10 2NA, UK

[2]Discovery Sciences, R&D, AstraZeneca, Gothenburg, 431 50, Sweden

[3]New Modalities and Parenterals Development, Pharmaceutical Technology and Development, Operations, AstraZeneca, Macclesfield, SK10 2NA, UK

[4]Functional Polymer Materials, Institute for Functional Materials and Biofabrication, Department of Chemistry and Pharmacy, Würzburg University, Röntgenring 11, 97070 Würzburg, Germany

[5]Soft Matter Chemistry, Department of Chemistry and Helsinki Institute of Sustainability Science, Faculty of Science, University of Helsinki, 00014 Helsinki, Finland

ABSTRACT

Polymeric micelles have been extensively used as nanocarriers for the delivery of chemotherapeutic agents aiming to improve their efficacy in cancer treatment. However, poor loading capacity, premature drug release, non-uniformity and reproducibility still remain the major challenges. To create a stable polymeric micelle with high drug loading, a telodendrimer micelle was developed as a nanocarrier for fulvestrant, as an example of a drug that has extremely poor water solubility (sub nanomolar range). Telodendrimers were prepared by synthesis of a hydrophilic linear poly(sarcosine) and growing a lysine dendron from the chain terminal amine by a divergent synthesis. At the periphery of the dendritic block, 4, 8, and 16 fulvestrant molecules were conjugated to the lysine dendron creating a hydrophobic block. Having drug as part of the carrier not only reduces the usage of the inert carrier materials but also prevent the drugs from leakage and premature release by diffusion. The self-assembled telodendrimer micelles demonstrated good colloidal stability (CMC < 2 μM) in buffer and were uniform in size. In addition, these telodendrimer micelles could solubilize additional fulvestrant yielding an excellent overall drug loading capacity of up to 77 wt.% total drug load (summation of conjugated and encapsulated). Importantly, the size of the micelles could be tuned between 25-150 nm by controlling (i) the ratio between hydrophilic and hydrophobic blocks and (ii) the amount of encapsulated fulvestrant. The versatility of these telodendrimer-based micelle systems to both conjugate and encapsulate drug with high efficiency and stability, in addition to possessing other tuneable properties makes it a promising drug delivery system for a range of active pharmaceutical ingredients and therapeutic targets.

INTRODUCTION

Polymeric micelles have served as highly promising platforms for the delivery of chemotherapeutic agents over the past three decades.[1] Chemotherapeutic agents often exhibit high toxicity and poor solubility which lead to a reduction in efficacy for cancer treatment. Micelles that are self-assembled from amphiphilic block copolymers (BCPs) and used as drug delivery systems can encapsulate hydrophobic drug molecules in the core whilst maintaining a hydrophilic corona on the surface providing high aqueous solubility and can control systemic exposure of the drug, reducing toxicity.[2-3] However, problems including low drug loading capacity and efficiency, poor colloidal stability in the bloodstream and rapid clearance, as well as non-uniform micelle size[4-5] still remain major challenges for the development of an effective micelle for drug delivery.[6-7] Physicochemical properties of a micelle such as shape, size, and surface chemistry have been reported to affect cell uptake, tumour penetration, and blood circulation time and have been identified as important determinants for the successful delivery of chemotherapeutic agents.[8-11]

The release of drugs from polymeric micelles is mainly affected by factors such as the diffusion coefficient of the drug, and the micelle's colloidal stability.[12] Micelle formulations undergo a large volume dilution following intravenous (i.v.) administration. When reaching a concentration below the critical micelle concentration (CMC), micelles should disassemble which should lead to increased drug release, unless they are kinetically trapped. This premature release of drug severely impacts the therapeutic performance of the drug delivery system.[6, 13] Although various types of micelles have been used in drug delivery, a system that can offer high levels of control over stability is still highly desirable.[14] From the extensive studies on polymeric micelles, researchers have identified the key factor that influences stability is the chemical composition of the core- and corona-forming blocks. Stability can be improved by increasing hydrophobic chain length and the degree of hydrophobicity. For example, Kabanov's group prepared a series of Pluronic micelles from block copolymers that differ in the lengths of the hydrophilic ethylene oxide (EO) and hydrophobic propylene oxide (PO) blocks. They found copolymers with higher content of hydrophobic block form micelles at lower concentration, i.e. exhibiting smaller CMC values.[15] Adams *et al*. synthesized poly(ethylene oxide)-*block*-poly(N-hexyl-$_{L}$-aspartamide) acyl conjugates with increasing acyl chain length on the hydrophobic block to form micelles. The increased side chain led to a similar reduction in CMC and resulted in more stable micelles.[16-17] Wishart's group investigated the effect of core hydrophobicity on micelle stability using some poly(ethylene

oxide)-*block*-peptide BCPs with different peptide sequences. Their findings suggested that BCPs synthesized from more aliphatic and aromatic peptides such as PEO-*b*-poly(phenylalanine) formed micelles of lower CMC values compared to those from PEO-*b*-poly(tyrosine).[18] This improvement in stability was a result of both increased hydrophobicity and π-π stacking interaction in the core. Other than π-π stacking,[19] hydrogen-bonding[20] and donor-acceptor coordination[21] have also been used to enhance core-drug interaction in order to improve micelle stability. Apart from micelle stability, the drug loading capacity and the increase of apparent drug concentration in the micelle can be considered as critical factors. Most drug delivery platforms, including polymeric micelles are often limited by drug loadings of less than 20 wt.% which can limit their applications as drug nanocarriers.[22] Increasing the hydrophobicity and binding affinity between the hydrophobic core-forming block and drugs has often been suggested to achieve high loading capacity.[7] On the other hand, some of the highest drug loadings for polymer micelles (exceeding 50 wt.%) have been reported using amphiphilic block copolymers[23-25] which have a minimal amphiphilic contrast or do not even form micelles in the absence of a drug.[26] Apart from drug formulations, polymer-drug conjugates (polymer prodrugs) are a popular alternative to cope with poorly soluble drugs and/or uncontrolled drug release. An interesting combination of both approaches is the use of polymer micelles that self-assemble from polymer-drug conjugates for the solubilization of additional drug. These usually exhibit a high loading capacity contributed from both physically encapsulated drugs and covalently conjugated drugs. For instance, Allen and co-workers prepared docetaxel-loaded micelles from both poly(ethylene glycol)-*block*-poly(ε-caprolactone) (PEG-*b*-PCL) and docetaxel (DTX) conjugated PEG-*b*-PCL(2k1k)-DTX.[27] The conjugated micelles showed up to 9.2 mg/mL DTX at a PEG-b-PCL(2k1k)-DTX concentration of 30 mg/ml, equivalent to an 1840-fold increase in aqueous solubility of DTX and the CMC of the PEG-*b*-PCL was reduced from 20.6 to 14.0 mg/L following the conjugation of DTX.

Here, a poly(sarcosine)-*b*-poly(L-lysine) based telodendrimer micelle is reported for the first time. Linear poly(sarcosine) (PSar) was polymerized from a primary amine initiator, and a poly(L-lysine) (PLL) dendron was divergently synthesized from the PSar chain terminal amino group. The resulting telodendrimer provided multiple functional sites at the dendritic ends for drug conjugation. Moreover, the linear-dendritic structure has been previously reported to provide enhanced core hydrophobicity to increase micelle stability as well as drug loading.[28-29] These telodendrimers were found to form uniform micelles in water *via* the co-solvent evaporation method.[22, 30] The conjugated fulvestrant on the telodendrimer formed the

hydrophobic core and was capable of encapsulating further fulvestrant. A series of micelles with controlled size (25 to 150 nm) and narrow size distribution were prepared by varying telodendrimer generation and drug feeding concentrations. Importantly, the conjugation of fulvestrant to the dendritic core-forming block not only increased the loading capacity of the encapsulated drug, but also minimized the drug release caused by diffusion. In combination with the good solubility and colloidal stability in water, these telodendrimers demonstrated great potential as nanocarriers for the delivery of fulvestrant.

MATERIALS AND METHODS

All reagents were purchased from Sigma-Aldrich unless stated otherwise. Z-Sar-OH was purchased from Fluorochem Ltd. Boc-L-Lys(Boc)-ONp was purchased from Chem-Impex International. Tert-butyl hydrogen succinate was purchased from Alfa-Aesar. 4-(4,6-Dimethoxy-1,3,5-triazin-2-yl)-4-methylmorpholinium tetrafluoroborate (DMTMM·BF_4) was synthesized as previously reported.[31] Sarcosine N-carboxyanhydride (NCA) was supplied from WuXi AppTec and further purified by crystallization from EtOAc/heptane prior to use.

Instrumentation

Nuclear Magnetic Resonance. ^{1}H NMR experiments were performed on a Bruker UltraShield AVIII 500 MHz spectrometer fitted with a QCI cryoprobe. All the measurements were conducted at room temperature using an acquisition time of 12 seconds and a delay time of 77 seconds to allow the full capture of polymer signals. Spectra were analysed using MestReNova version 9.0.

Multi Detector Size Exclusion Chromatography (MD-SEC). Size exclusion chromatography (SEC) was performed on a Malvern Panalytical OMNISEC system using two PSS Novema Max columns (100 Å (10 µm) + 30 Å (5 µm)) in series with an aqueous eluent of 100 mM NaCl + 0.1 v/v% TFA. The system was calibrated using a single PEO narrow standard (24 kDa, dn/dc = 0.132) and absolute molar masses were determined using the refractive index (RI) and light scattering signals. Samples were prepared at 2-5 mg/mL and analyzed using OMNISEC software version 11.0.

Matrix-Assisted Laser Desorption/Ionization Time of Flight Mass Spectrometry. MALDI-TOF was performed on a Bruker UltrafleXtreme using the built-in method LP_5-20kDa. Samples were prepared at 5 mg/mL in methanol. A 1:1 (v/v) mixture of matrix solution and sample solution were spotted onto an MTP 384 polished steel target plate (1µL, twice per spot). α-CHCA matrix solution (saturated in 50% ACN/0.1% aqueous TFA) was used for linear PSar

and super-DHB matrix solution (40 mg/mL in THF) was used for telodendrimers. Spectra were recorded using Bruker flexControl software version 3.4 and analyzed by Bruker flexaAnalysis software version 3.4.

Dynamic Light Scattering. A Malvern Zetasizer® Ultra instrument equipped with multi-angle detector (173°, 13°, and 90°) and He-Ne laser at wavelength 633 nm was used for both size measurement and CMC determination. The dispersant RI and viscosity of water were used (n = 1.59 and η = 0.888 mPa·s). Samples were filtered through a 0.45 µm PVDF syringe filter prior to measurement. All the experiments were conducted at 25 °C in triplicate, using three individually prepared samples and results are presented as mean ± standard deviation (SD). Data were obtained using ZS XPLORER software version 1.0.

Mass Photometry. Mass photometry was performed on a Refeyn One mass photometry instrument (Refeyn Ltd, UK). All the micelle samples were diluted to 4 µg/mL in HBS-N (10 mM HEPES, 150 mM NaCl, pH = 7.4) and analyzed using 60 s acquisition time. Peak contrast was calculated from the resulting histograms using Gaussian fits. As scattering signal scales with polarizability, which is a function of refractive index and proportional to particle volume, the contrast-to-mass conversion was achieved using a native protein ladder with known species of different sizes (NativeMark, ThermoFisher). Despite differences in refractive index between proteins (dn/dc ~0.185) and PSar star polymers (dn/dc ~0.16), previous characterization of PSar star polymers using MP have shown that masses obtained for the star polymers are in good agreement with both MD-SEC and MALDI-TOF-MS.[32]

Methods

Synthesis of linear poly(sarcosine)

Sarcosine NCA (2.16 g, 18.2 mmol) was fully dissolved in 12 mL of anhydrous DMF under nitrogen protection. The initiator 2-methoxyl ethyl amine (16 µL, 0.183 mmol), dissolved in 1 mL of DMF was added rapidly to the monomer solution via a syringe. The reaction mixture was stirred for 4 h at room temperature with nitrogen flow. The solution was slowly added to a rapidly stirring tert-butyl methyl ether (TBME) (200 mL) to form a precipitate. The precipitate was collected *via* vacuum filtration and dried overnight at 40 °C in a vacuum oven. Yield 1.27 g, 96.4%. GPC see Figure 1. ^{1}H NMR see Figure S1 in ESI. Molecular weight data see Table 1.

Synthesis of poly(sarcosine)-b-poly(L-lysine) telodendrimer $PSar_{100}$-b-$PLL[NH_2.TFA]_n^{Gm}$

A series of amide coupling reactions were employed to generate poly(sarcosine)-*b*-poly(L-lysine) telodendrimer $PSar_{100}$-*b*-$PLL[NH_2.TFA]_n^{Gm}$ of desired generation. The 1st generation $PSar_{100}$-*b*-$PLL[NH.Boc]_2^{G1}$ was prepared by coupling Boc-L-Lys(Boc)-ONp (120 mg, 0.254 mmol, 2 equiv.) on to the *N*-terminus of linear $PSar_{100}$ (850 mg, 0.118 mmol) in anhydrous DMF (5 mL). The reaction mixture was stirred for 4 h under nitrogen protection and then slowly added to a rapidly stirring TBME (200 mL) to form a precipitate. The solid was collected via vacuum filtration and dried overnight at 40 °C in a vacuum oven. Yield 846 mg, 95.2 %. To remove the Boc protecting group, $PSar_{100}$-*b*-$PLL[NH.Boc]_2^{G1}$ (820 mg) was dissolved in 8 mL DCM/TFA (1:1 by volume) and stirred for 2 hr at room temperature under nitrogen. The reaction mixture was added dropwise to a rapidly stirring TBME (200 mL) to precipitate. The resulting $PSar_{100}$-*b*-$PLL[NH_2.TFA]_2^{G1}$ was collected via vacuum filtration and dried overnight at 40 °C in a vacuum oven. Yield 817 mg, 99.2 %. The 2nd to 4th generation $PSar_{100}$-*b*-$PLL[NH_2.TFA]_n^{Gm}$ telodendrimers were prepared following the same method.

Synthesis of fulvestrant succinate

Fulvestrant (100 mg, 0.16 mmol) was added to a 25-mL round bottom flask and dissolved in 3 mL anhydrous DCM under nitrogen, followed by the addition of triethylamine (TEA) (2 equiv.), 4-dimethylaminopyridine (20 mg, 0.16 mmol), EDC·HCl (80 mg, 0.4 mmol), and tert-butyl hydrogen succinate (30 mg, 0.17 mmol). The reaction was left to stir at room temperature and followed to completion by UPLC-MS (approximately 1 hr). The reaction mixture was diluted with DCM (20 mL) and washed with 0.2 M HCl (20 mL, twice) followed by brine (20 mL). The organic layer was dried over magnesium sulfate. The solvent was removed under vacuum and yielded 112 mg, 89% fulvestrant t-butyl succinate. To remove the tert-butyl ester protecting group, TFA/DCM (3 mL, 1:1 by volume) were added to fulvestrant t-butyl succinate and stirred under nitrogen for 2 h. The excess solvent and t-butyl alcohol by-product were removed by rotary evaporation. The product fulvestrant succinate was obtained as a clear oily liquid, yield 96 mg, 92.5%. For ^{1}H NMR spectra, see Figure S2.

Synthesis of fulvestrant conjugated telodendrimer $PSar_{100}$-b-$PLL[FLV]_8^{G3}$ (TD-FLV8)

Fulvestrant succinate (96 mg, 0.136 mmol) and 4-(4,6-dimethoxy-1,3,5-triazin-2-yl)-4-methyl-morpholin-4-ium (71 mg, 0.216 mmol) were added to a 10-mL round bottom flask and completely dissolved in 1 mL anhydrous DMF. In a separate vial, $PSar_{100}$-*b*-$PLL[NH_2.TFA]_8^{G3}$ (112 mg, 0.0125 mmol) was dissolved in 1.5 mL anhydrous DMF. After adjusting the pH to ~8 using TEA, $PSar_{100}$-*b*-$PLL[NH_2.TFA]_8^{G3}$ solution was transferred to the mixture and stirred at room temperature for 3 hr. The reaction mixture was slowly added to rapidly stirring TBME

(100 mL) to form a precipitate. The precipitate was collected and purified by centrifugation (3900 g, 5 min, repeated 3 times) to give a white solid. The solid was dried overnight under vacuum at 40 °C . Yield 111 mg, 67.1%.

$PSar_{100}$-*b*-$PLL[FLV]_4^{G2}$ (TD-FLV4) was prepared using the same method. Reagent quantities: fulvestrant succinate (800 mg, 1.0 mmol), 4-(4,6-dimethoxy-1,3,5-triazin-2-yl)-4-methyl-morpholin-4-ium (450 mg, 1.372 mmol), $PSar_{100}$-*b*-$PLL[NH_2.TFA]_4^{G2}$ (400 mg, 0.0366 mmol), and 7 mL anhydrous DMF. Yield 583 mg, 79.2%.

$PSar_{100}$-*b*-$PLL[FLV]_{16}^{G4}$ (TD-FLV16) was prepared using the same method. Reagent quantities: fulvestrant succinate (140 mg, 0.158 mmol), 4-(4,6-dimethoxy-1,3,5-triazin-2-yl)-4-methyl-morpholin-4-ium (76 mg, 0.231 mmol), $PSar_{100}$-*b*-$PLL[NH_2.TFA]_{16}^{G4}$ (151 mg, 0.0188 mmol), and 2 mL anhydrous DMF. Yield 182 mg, 93.7%.

Preparation of telodendrimer micelles

Both blank and drug-encapsulating telodendrimer micelles were prepared by co-solvent evaporation method. A unimer solution was prepared by dissolving the telodendrimer and various amount of fulvestrant (drug feeding of 0 to 50 wt.%) in acetone to give a final concentration of 20 mg/mL. The unimer solution was added dropwise to an equal volume of water. The mixture solution was stirred briefly for 5 min and then the acetone was evaporated under nitrogen using a Smart Evaporator (BioChromato, Japan). The complete removal of acetone was monitored by ^{1}H NMR. The resulting micelle solutions were filtered through a 0.45 μm filter to remove any larger aggregates. Quantification of fulvestrant was conducted using ^{1}H NMR (Figure S7-S10). Telodendrimer and fulvestrant were weighed out at each planned feeding ratio and dissolved in *d*-acetic acid for proton NMR measurements to determine the integrations of conjugated fulvestrant and free fulvestrant. After drug encapsulation, the filtered micelle solutions were freeze dried and re-dissolved in *d*-acetic acid for proton NMR measurements to determine the amount of encapsulated fulvestrant, using the conjugated fulvestrant as internal reference. A purity check by proton NMR for TD-FLV8 telodendrimer was performed using maleic acid as reference standard in order to accurately determine the feeding fractions for each fulvestrant-encapsulating micelles (Figure S7).

The drug encapsulation efficiency (EE%) and loading capacity (LC%) were calculated using the following equations:

$$\text{EE \%} = \frac{m_{drug}}{m_{drug\ added}} \times 100\%$$

$$\text{LC \%} = \frac{m_{drug}}{m_{polymer}+m_{drug}} \times 100\%$$

where m_{drug} and $m_{polymer}$ are the weights of the drug and telodendrimer in the micelle, and $m_{drug,added}$ is the initial mass of the drug added.

The total drug loading capacity including both chemically conjugated and physically encapsulated drugs was calculated using the following equation:

$$\text{LC}_{\text{total}}\ \% = \frac{m_{drug}+ x \times m_{polymer}}{m_{polymer}+m_{drug}} \times 100\%$$

where *x* is the wt. % of the conjugated fulvestrant in each telodendrimer as shown in Table 3.

CMCs of telodendrimer micelles

The CMCs of both blank and drug-encapsulating micelles in PBS buffer were estimated by dynamic light scattering. The micelle samples were prepared by serial dilution and concentration varied from 0.01 to 100 μg/mL. The intensity of scattered light in kilo-counts per second (kcps) was measured using a fixed attenuator at 11 for all the micelle solutions. To determine the CMC, the intensity was plotted against concentration and the intersection of the two slopes indicated the onset of micellization.

Hydrolysis-induced drug release from the micelles

The release of fulvestrant from blank TD-FLV8 micelles was performed at 37 °C in PBS buffer at pH 5.5, pH 7.4, and pH 8.5. In addition, the effect of protein binding on drug release was tested at pH 7.4 using 45 mg/mL bovine serum albumin (BSA). Typically, 1 mL micelle solution (2 mg/mL) was incubated at 37 °C with gentle stirring. Fulvestrant released from the micelles precipitated in solution due to its poor solubility. Aliquots of 50 μL were taken at various time points and then mixed with 50 μL acetonitrile to completely solubilize the released fulvestrant. To ensure the drug was suspended homogenously, the solution was sonicated for 5 min before taking each aliquot. The amount of drugs released was assessed by UPLC using a standard calibration curve of fulvestrant as shown in Figure S13. The percentage of drug release from telodendrimer micelles were summarized in Table S1.

RESULTS AND DISCUSSION

Preparation and Characterization of $PSar_{100}$-b-$PLL[NH_2.TFA]_n^{Gm}$ Telodendrimer.

A telodendrimer is an amphiphilic block copolymer that has a linear block and a dendritic block.[33] Its unique linear-dendritic structure has demonstrated enhanced polymer-drug interactions, making the telodendrimer micelle a very promising nanocarrier for drugs.[28] Some

PEG-containing telodendrimer micelles have been used to encapsulate insoluble drugs, however, achieving high loading capacity and uniform micelle size have always been challenging.[28-29, 34] Here, a PSar-based telodendrimer micelle system was specifically designed for the poorly soluble fulvestrant, an oestrogen receptor antagonist that has been widely used to treat hormone receptor-positive metastatic breast cancer. Fulvestrant has extremely poor water solubility and is dosed as a sterile oily solution *via* intramuscular injection in order to give adequate bioavailability.[35] Using telodendrimer micelle to deliver fulvestrant provides many advantages compared to traditional linear block copolymer micelles. For instance, the dendritic block in telodendrimer helps form well-defined architecture with narrow dispersity. Moreover, drugs can be loaded into the dendritic micelle core *via* both chemical conjugation and physical encapsulation to achieve high loading capacity. In the present design, a PSar homopolymer with a chain length of 100 repeat units was synthesized as the linear block and PLL dendrimers of various generations were grown from the chain end to form the dendritic block (Scheme 1). The corona-forming PSar is a promising replacement for the most widely used PEG due to its high hydrophilicity, biocompatibility and low antigenicity.[36-39] $PSar_{100}$ was synthesized using nucleophilic ring-opening polymerization of sarcosine NCA using 2-methoxyl ethyl amine as the initiator. The resulting polymer was fully characterized by ^{1}H NMR, MD-SEC, MALDI-TOF (Figure S1, Figure 1b and 1c), and its key properties are summarized in Table 1.

The terminal secondary amine of PSar was used as the focal point for the synthesis of the PLL dendritic block. Through a series of nucleophilic addition/elimination reactions using Boc-*L*-Lys(Boc)-ONp followed by Boc-deprotection, poly(sarcosine)-*b*-poly(L-lysine) ($PSar_{100}$-*b*-$PLL[NH_2.TFA]_n^{Gm}$) telodendrimers of the different generations could be synthesized (Table 1). As shown in Figure 1a, ^{1}H-NMR analysis of the Boc-protected telodendrimer $PSar_{100}$-*b*-$PLL[NH.Boc]_n^{Gm}$ was used to confirm the full conversion (with the analytical limitation) of each generation when comparing the protons of the Boc groups on the dendritic block (1.47 ppm) to the -CH_2- signal (4.1-4.6 ppm) from the sarcosine repeat units. Trace amount of washing solvent TBME was left in the sample and showed two singlets at 3.30 ppm and 1.25 ppm. Analysis of the $PSar_{100}$-*b*-$PLL[NH_2.TFA]_n^{Gm}$ telodendrimers by MD-SEC and MALDI-TOF-MS (Figure 1b and 1c) yielded molar masses that were consistent with results obtained from ^{1}H-NMR. All of the telodendrimers prepared following this method exhibited narrow molar mass distributions ($Đ < 1.10$) and precise control over size and generation, i.e. number of amine end groups, and therefore sites for subsequent drug

conjugation. The only exception is $PSar_{100}$-*b*-$PLL[NH_2.TFA]_{16}^{G4}$ telodendrimer, whose molar mass determined by MD-SEC (Figure 1b) was lower compared with that obtained from ^{1}H-NMR and MALDI-TOF-MS. This lower apparent molecular weight suggested the 4th generation telodendrimer experienced some degradation during the TFA deprotection.

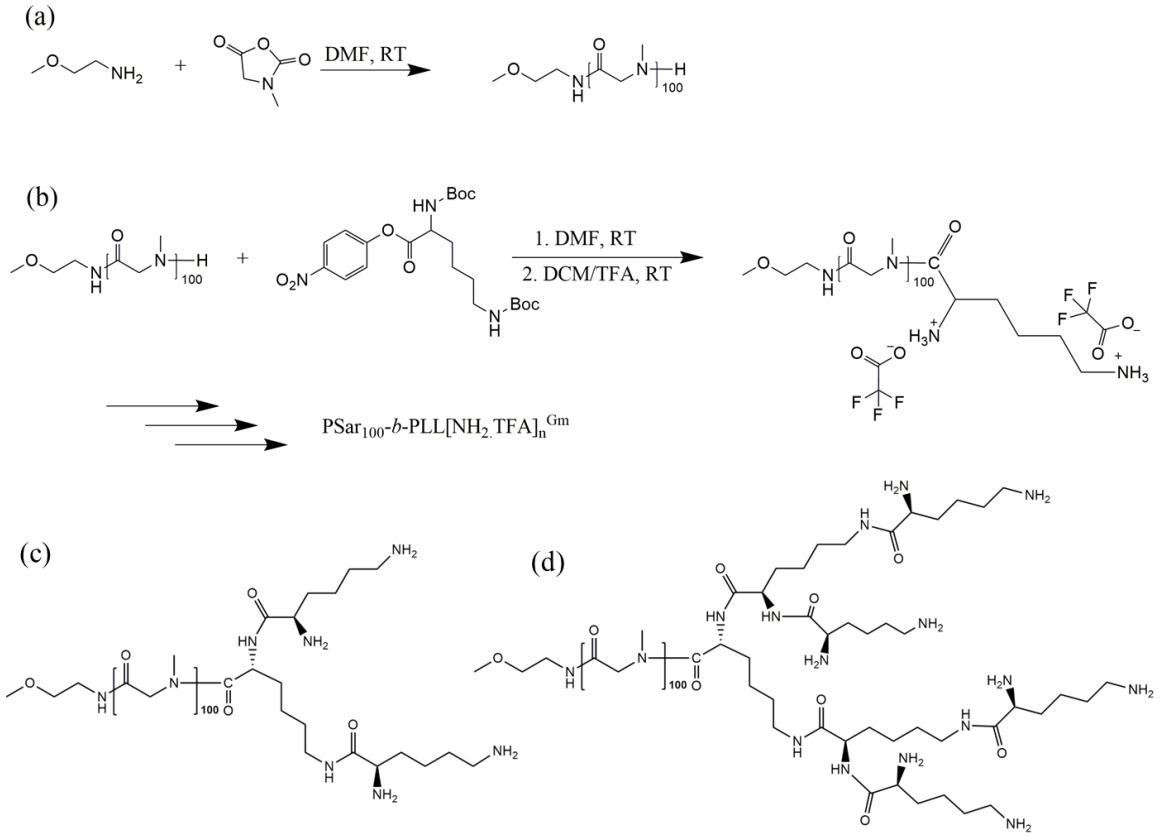

Scheme 1. Synthesis of (a) linear PSar and (b) telodendrimer of mth generation that contains *n* number of amines. Chemical structures of (c) 2nd and (d) 3rd generation telodendrimers.

Table 1. Characterization of PSar linear polymer and telodendrimers of different generations

Samples	**M_n[a]**	**Đ[a]**	**DP[b]**	**M_P[c]**
$PSar_{100}$	7.1	1.01	100	6065
$PSar_{100}$-*b*-$PLL[NH_2.TFA]_2^{G1}$	5.8	1.05	106	6193
$PSar_{100}$-*b*-$PLL[NH_2.TFA]_4^{G2}$	6.9	1.05	88	6520
$PSar_{100}$-*b*-$PLL[NH_2.TFA]_8^{G3}$	7.0	1.08	98	7038
$PSar_{100}$-*b*-$PLL[NH_2.TFA]_{16}^{G4}$	6.8	1.15	90	7782

[a] MD-SEC (kDa). [b] Degree of polymerization from ^{1}H NMR. [c] Peak maximum m/z from MALDI-TOF.

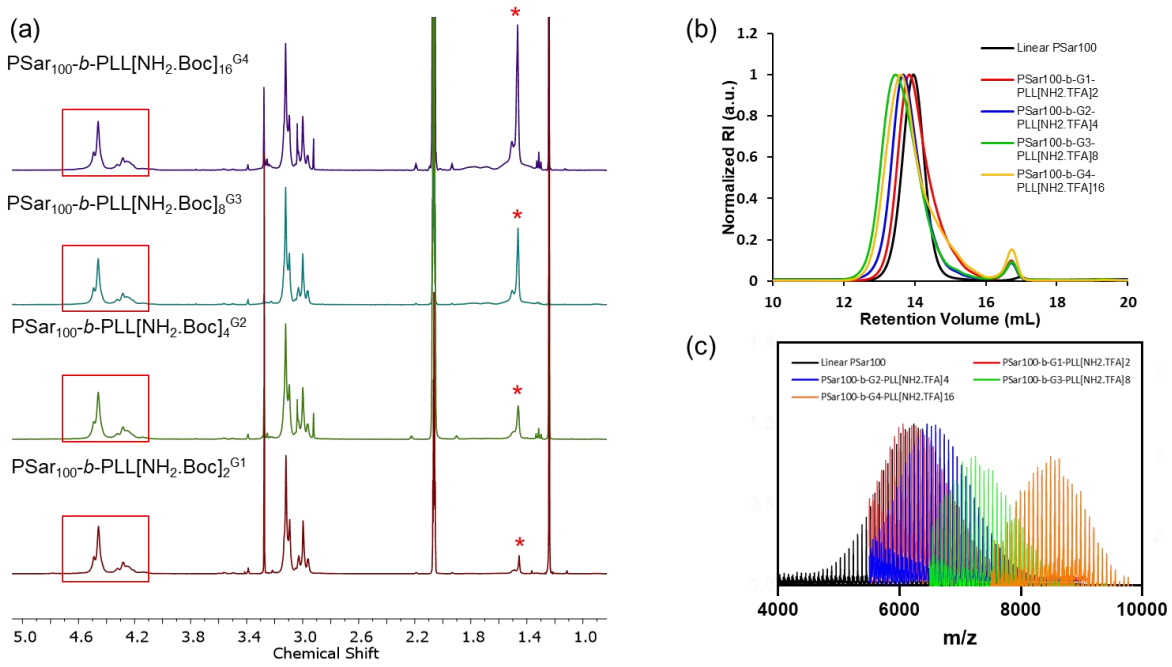

Figure 1. Characterization of $PSar_{100}$-*b*-$PLL[NH_2.TFA]_n^{Gm}$ telodendrimers from G1 to G4. (a) ^1H NMR spectra (d_4-acetic acid) of $PSar_{100}$-*b*-$PLL[NH.Boc]_n^{Gm}$ telodendrimers highlighting signals from (*) Boc on the lysine dendron and (□) PSar (methylene groups). (b) Aqueous SEC chromatograms showing the normalized RI signals and (c) MALDI-TOF spectra from linear $PSar_{100}$ and $PSar_{100}$-*b*-$PLL[NH_2.TFA]_n^{Gm}$ telodendrimers G1 to G4.

Synthesis of fulvestrant-conjugated telodendrimer.

To induce amphiphilicity in the telodendrimers, the hydrophobic drug molecule fulvestrant was conjugated to the amino groups at the periphery of the dendritic block. Fulvestrant was first modified by attachment of a succinic acid linker to enable direct conjugation to the telodendrimer lysine amines *via* amide coupling. The synthetic procedures employed for the preparation of fulvestrant-conjugated telodendrimer $PSar_{100}$-*b*-$PLL[FLV]_n^{Gm}$ ($TD\text{-}FLV_n$) are shown in Scheme 2.

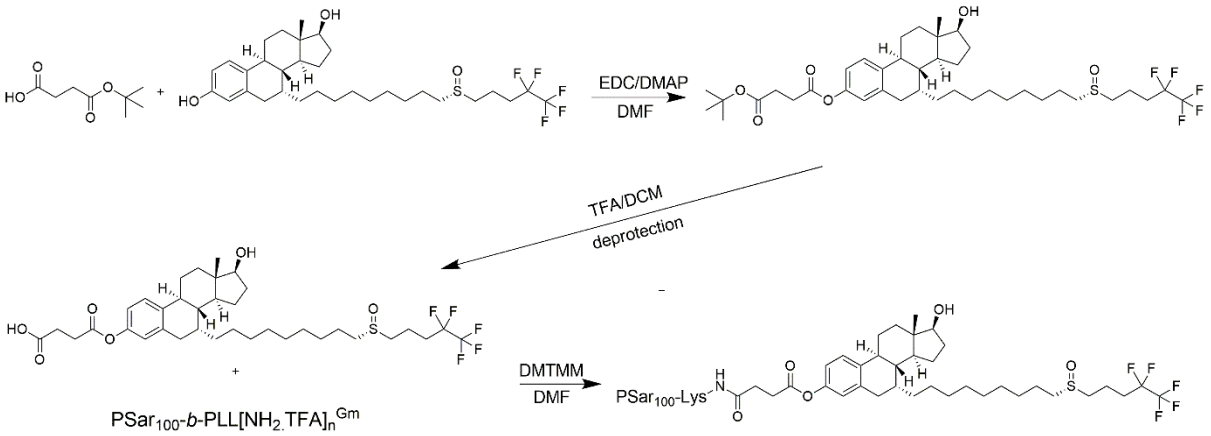

Scheme 2. Synthesis of fulvestrant succinate and conjugation to telodendrimer to form $PSar_{100}$-*b*-$PLL[FLV]_n^{Gm}$.

Fulvestrant has two hydroxyl groups at the 3 and 17 positions available for functionalization. Due to the increased reactivity and lower pKa of the phenol, the esterification with *t*-butyl succinate preferentially took place at the 3 position and yielded mono-substituted fulvestrant *t*-butyl succinate. The *t*-butyl protecting group was removed using TFA/DCM to yield fulvestrant succinate. As outlined in Figure S2, the disappearance of the singlet at 1.5 ppm in ^{1}H NMR spectra confirmed the complete removal of the *t*-butyl protecting group and left a carboxylic acid functional group available for conjugation to the telodendrimer. Figure 2 shows the chemical structure and ^{1}H-NMR spectrum of a 3rd generation fulvestrant-conjugated telodendrimer PSar$_{100}$-*b*-PLL[FLV]$_{8}^{G3}$ (TD-FLV8) with 8 fulvestrant molecules attached at the periphery of the dendritic block. Peaks *a* (4.1-4.6 ppm, 200H, CO-*CH$_2$*-N) and *b* (3.35 ppm, 3H, *CH$_3$*-O) were assigned to the linear PSar block indicating a chain length of ~100 repeat units. The appearance of peaks (*d*, *e*, and *f*) in the aromatic region confirmed the successful conjugation of fulvestrant to the telodendrimer. Ratios of fulvestrant to PSar were determined from the integration of peak e and peak *a*. On average, ~6.5 fulvestrant molecules were attached to each PSar chain. In addition to TD-FLV8, a 2nd generation TD-FLV4 and a 4th generation TD-FLV16 drug-conjugated telodendrimer were also synthesized and characterized following the same method (Figure S3) to carry 4 and 16 fulvestrant molecules at the dendritic block, respectively. MALDI-TOF-MS measurements were performed on TD-FLV4 and TD-FLV8 and confirmed the molecular weights of these drug-conjugated telodendrimers were consistent with the theoretical values (Figure S4).

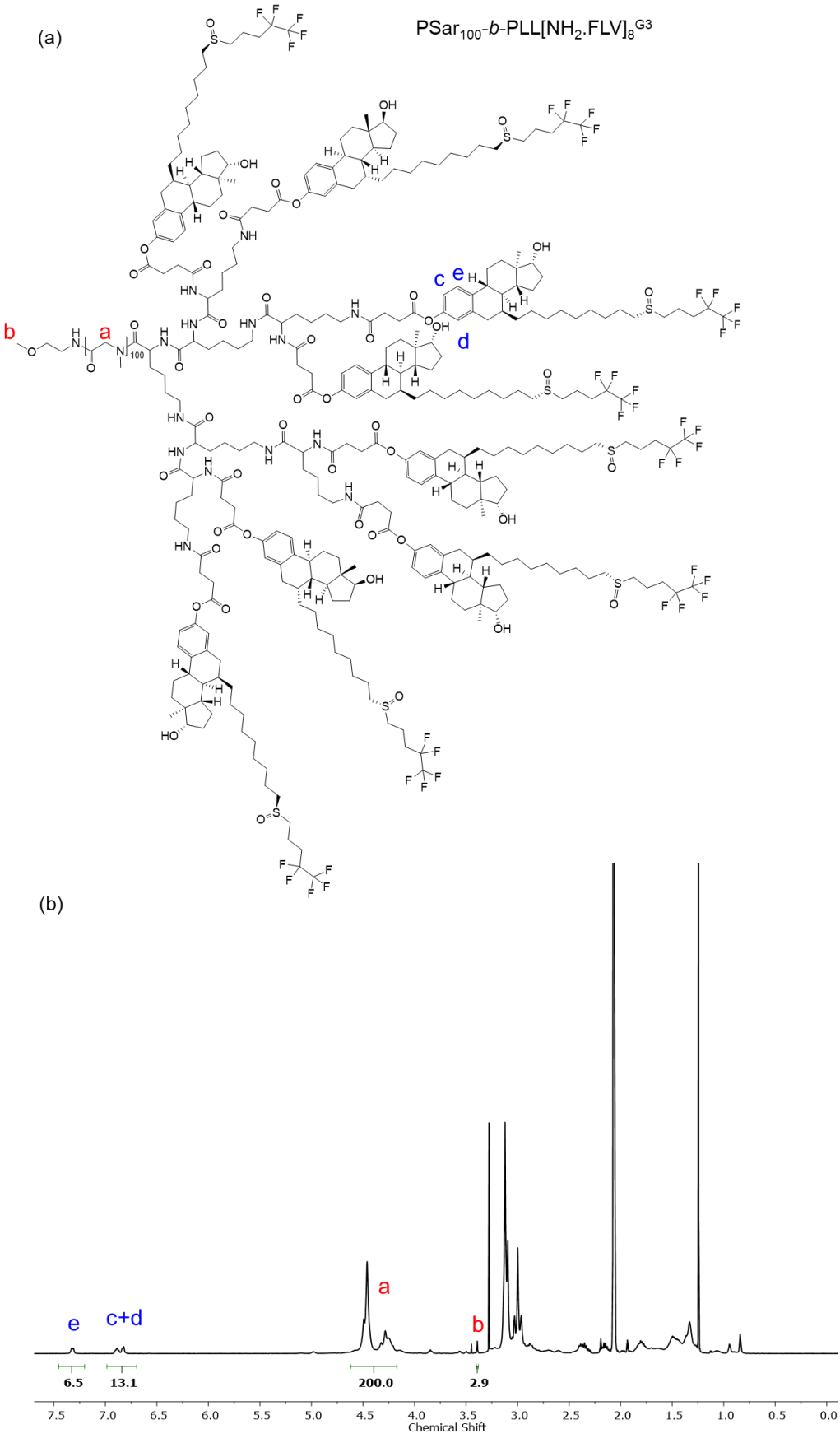

Figure 2. (a) Chemical structure of $PSar_{100}$-*b*-$PLL[FLV]_8^{G3}$ (TD-FLV8) and (b) ^1H NMR (500 MHz, d4-AcOH, 300 K) spectrum with corresponding peak assignments.

Self-assembly of fulvestrant-conjugated telodendrimers.

Telodendrimer micelles were prepared in water from all TD-FLV$_n$ (n = 4, 8, 16) samples by using a co-solvent evaporation method.[22] The fulvestrant-conjugated telodendrimers were dissolved in acetone to prepare concentrated unimer solutions of 20 mg/mL. The unimer solution was then slowly added to an equal volume of water with rapid stirring, followed by evaporation of the organic solvent under reduced pressure. The highly hydrophobic fulvestrant in the dendritic block triggered the formation of micelle to minimize the interfacial energy. The resulting micelles were characterized using dynamic light scattering (DLS) to obtain the average hydrodynamic size and polydispersity as summarized in Table 2. The micelle sizes were found to depend on the telodendrimer generation. As the generations increased from 2 to 4, the mass ratio of hydrophobic/hydrophilic blocks increased from 23/77 to 48/52. As shown in Figure 3a, the DLS results of the 2nd generation TD-FLV4 micelle gave an average size of 25 ± 0.8 nm with a polydispersity index (PDI) of 0.15. As the number of fulvestrant molecules on the dendritic block increased from 4 to 8, the 3rd generation TD-FLV8 micelle exhibited a slightly larger size of 30 ± 0.7 nm with PDI = 0.07. A more significant increase to 116 ± 2.8 nm (PDI = 0.18) was observed for the 4th generation TD-FLV16 micelle, with 16 fulvestrant molecules on the dendritic block. Interestingly, the change in size was much more significant in micelles formed from telodendrimers of high generations than those made of low generations. Only a 5 nm increase was observed when the number of fulvestrant molecules doubled from TD-FLV4 to TD-FLV8, whereas a 4 times increase in size was observed for TD-FLV16 compared to TD-FLV8 micelles. This drastic increase in size might be a result of morphology change away from a simple micelle structure, which could be explained by the expansion of hydrophobic block volume in addition to the increased block length due to the presence of more fulvestrant molecules. Indeed preliminary CryoEM studies indicated these larger structures were polymersomes as shown in Figure S5. The changes in size caused by increasing the hydrophobic to hydrophilic block ratio were also found much more significant in telodendrimers than in linear block copolymers as the dendritic hydrophobic block is much more localised compared with the linear hydrophobic block of similar molecular weight.[33, 40]

Another self-assembly method, thin-film dissolution was also explored to prepare TD-FLV$_n$ micelles. Though it is a very commonly used technique for the formation of micelles, we only had limited success with TD-FLV4. Figure S6 includes the hydrodynamic size distributions of TD-FLV4 micelles prepared using co-solvent evaporation and thin-film methods. Larger structures of 56 nm with slightly higher polydispersity of 0.17 were obtained

using the latter method. In the thin-film self-assembly experiments, when water was added to rehydrate the telodendrimer film, all three TD-FLV$_n$ samples formed needle-like crystals in solution which were difficult to fully disperse even upon sonication. The re-hydrated solutions were left at room temperature for 1 week. Only the solution containing TD-FLV4 turned clear suggesting the formation of micelles as revealed by DLS, whereas TD-FLV8 and TD-FLV16 solutions still contained large precipitates at the bottom.

The difference between TD-FLV4 micelle size caused by different self-assembly pathways can be attributed in part to the different microenvironment the telodendrimers were exposed to during micelle formation. In the co-solvent evaporation method, the telodendrimer was dissolved in mixtures of organic and aqueous solvents and the organic solvent was then slowly removed. In this scenario, it is thought that the telodendrimers were given enough time to reach an equilibrium and form micelles from a homogenous starting point during the slow evaporation. Whereas in the thin-film approach, the hydrated telodendrimer film initially formed micelles, or much larger structures with broad size distribution and then underwent sonication to produce more uniform and smaller micelles. The telodendrimer chains are likely to have low mobility in aqueous solution due to the highly insoluble fulvestrant molecules on the dendritic block. Therefore, micelles formed in this way could not reach the thermodynamic equilibrium and resulted in larger sizes as well as broader size distributions. The difficulties in preparing TD-FLV8 and TD-FLV16 micelles using the thin-film approach could be explained using the same line of argument. As the number of fulvestrant molecules on the dendritic block increased to 8 and 16, the solubility or mobility of these telodendrimers decreased drastically in aqueous solvent. Therefore the telodendrimers tended to form kinetically trapped agglomerates and precipitate by thin-film hydration.

Encapsulation of additional fulvestrant using the TD-FLVn micelles

Poor drug loading has been a major limitation in polymer micelle delivery systems and only few types of micelles can achieve a loading capacity >20 wt.%.[22-23, 26, 41-43] Since polymer-drug interaction is the driving force for the formation of drug encapsulated micelles, we hypothesize that using the drug itself as a binding moiety within the telodendrimer structure could provide the maximum interaction and thus lead to high loading. The fulvestrant molecule contains an aromatic head group with a long hydrocarbon chain as well as 2 hydrogen bond donors and 3 acceptors which can provide a π-π interaction, hydrophobic interaction and hydrogen bonding respectively. Moreover, the unique fluorophilic domain in fulvestrant molecule can probably drive the self-assembly in aqueous environment even further as it

reduces self H-bonding and increases fluorocarbon self-assembly. The co-solvent evaporation method was employed to prepare drug encapsulated telodendrimer micelles. The fulvestrant loading capacity of TD-FLV$_n$ (n = 4, 8, and 16) micelles was compared and summarized in Table 2. Similarly, to the preparation of blank micelles, TD-FLV$_n$ was mixed with fulvestrant of various feeding concentrations to give a total concentration of 20 mg/mL in acetone. The telodendrimer/drug mixture solution was added to water of equal volume and formed micelles upon evaporation of organic solvent. Non-encapsulated fulvestrant was removed using a 0.45 µm syringe filter and the micelle solutions obtained were completely clear. ^{1}H NMR was used to determine both the drug loading capacity (LC) % and encapsulation efficiency (EE) % of these micelles. Figure S8-S10 show the ^{1}H-NMR spectra of TD-FLV$_n$ micelles with their maximum loadings. The aromatic proton signals (6.25 – 7.25 ppm) from fulvestrant broadened and shifted downfield when conjugated to the telodendrimer. Therefore, it was possible to integrate both conjugated and encapsulated drug and therefore calculate the amount of fulvestrant physically encapsulated in the micelle. Similarly, the encapsulation efficiency can be determined by comparing the amount of physically encapsulated fulvestrant before and after the self-assembly process. Detailed characterizations of these fulvestrant encapsulated micelles are summarized in Table 2 and Figure 3. The TD-FLV4 micelle showed a maximum loading capacity of 5 wt.% fulvestrant with a micelle size increase from 25 to 32 nm. An EE of 98.8% was achieved for this micelle, multiple peaks were observed in the DLS, indicating a heterogenous size distribution. Fulvestrant loading capacity was found to increase with dendron generation. The 3rd generation TD-FLV8 micelle had a maximum LC of 31 wt.% (EE = 98.0%) while the 4th generation TD-FLV16 micelle showed an even higher LC of 57 wt.% (EE = 77.8%). In addition to the physically encapsulated drugs, there was also a contribution of drug loading from the covalently conjugated fulvestrant on dendritic block. Therefore, the maximum total drug contents for TD-FLV8 and TD-FLV16 were an impressive 57 wt.% and 77 wt.%, respectively.

The TD-FLV$_n$ self-assemblies also demonstrated excellent aqueous solubility. To find the maximum solubility of fulvestrant in water, a TD-FLV8 micelle solution was concentrated using a centrifugal spin-filter device with a 30 kDa molecular weight cut-off membrane to obtain a final micelle concentration of 100 mg/mL, whilst still being a fluid solution. However, the micelle solution became viscous at this point and was difficult to concentrate further. Fulvestrant has very poor solubility in water (9.53 ng/L).[44] However, using these telodendrimer

micelles it was possible to increase the effective solubilization of the drug to ~57 g/L in water, which is a ~10^9-fold increase.

Table 2. Summary of characteristics and fulvestrant encapsulation data for different TD-FLV telodendrimer micelles

Telodendrimer	**MW[a] (kDa)**	**Conjugated FLV[a] (wt.%)**	**Size[b] (nm)**	**PDI[b]**	**LC%[c]**	**EE%[c]**	**LC_{total} %**
$PSar_{100}$-*b*-$PLL[FLV]_4^{G2}$	10.3	23	25 ± 0.8	0.15	-	-	23
			multiple	n/a	5	98.8	27
$PSar_{100}$-*b*-$PLL[FLV]_8^{G3}$	13.3	36	30 ± 0.7	0.07	-	-	36
			40 ± 0.5	0.15	18 ± 1.0	99.6 ± 4.3	44
			47 ± 0.4	0.09	28 ± 0.8	99.3 ± 2.7	51
			53 ± 3.8	0.09	31 ± 1.1	98.0 ± 4.9	53
			60 ± 5.9	0.08	37 ± 1.7	68.2 ± 4.6	57[d]
$PSar_{100}$-*b*-$PLL[FLV]_{16}^{G4}$	20.3	48	116 ± 2.8	0.18	-	-	48
			140 ± 1.8	0.13	40	63.5	69
			150 ± 4.5	0.12	56	77.8	77

[a] Theoretical molecular weight and conjugated drug content. [b] Hydrodynamic diameter and polydispersity index (PDI) obtained from DLS. [c] Loading capacity (LC) and encapsulation efficiency (EE) obtained from ^{1}H NMR. [d] Maximum micelle solubility was determined to be 100 g/L in water, equivalent to a fulvestrant concentration of 57 g/L, which represents an ~10^9-fold increase in the apparent water solubility of fulvestrant (9.53 ng/L). LC and EE of $PSar_{100}$-*b*-$PLL[FLV]_8^{G3}$ micelles were conducted using three individually prepared samples and results are presented as mean ± standard deviation (SD).

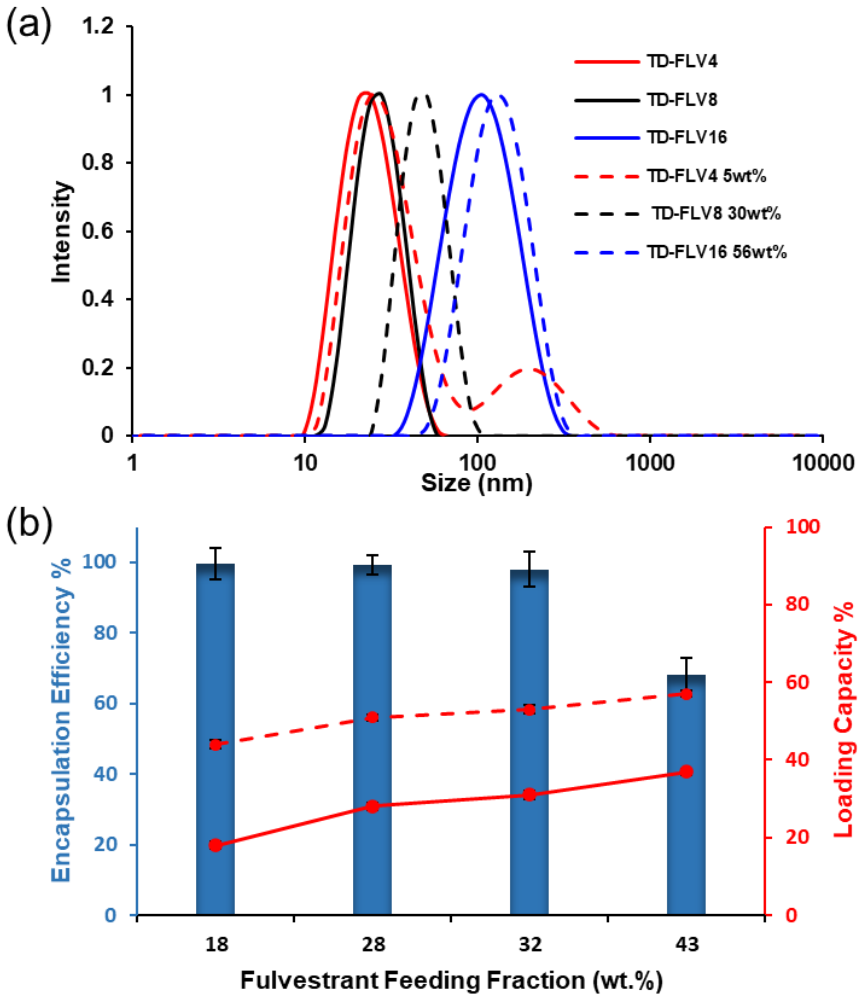

Figure 3. (a) Tuneable size ranges for micelles prepared from TD-FLV4 (red), TD-FLV8 (black), and TD-FLV16 (blue). Solid lines represent the sizes of blank micelles and dashed lines indicate the micelle size with maximum drug loading. (b) Encapsulation efficiency % and loading capacity % of TD-FLV8 micelles at various drug feeding concentrations. Solid red line: LC% of physically encapsulated drug, dashed red line: total fulvestrant content including both physical and covalently bound drug. Micelle concentration was kept at 20 mg/mL. All the experiments were conducted using three individually prepared samples and results are presented as mean ± standard deviation (SD).

To the best of our knowledge, such high loading capacity and solubility improvement of a drug are rarely seen for polymer micelle nanocarriers.[21, 25, 45] The excellent drug loading capacity of these TD-FLV$_n$ micelles can be attributed to the optimized drug binding ability obtained from using a fulvestrant-conjugated telodendrimer. The broad principle 'like dissolves like' suggests that an efficient binding molecule should have similar structural motifs and conformation as the drug in order to maximize the interaction. Considering this principle, one of the strongest candidates for matching the drug must be the drug itself.

Critical micelle concentration determination

In typical drug delivery applications, micelles will undergo extensive dilution after being injected into the bloodstream. When the concentration is below the critical micelle concentration (CMC), micelles will dissociate. As such, a stable micelle with low CMC can reduce the premature drug release caused by the destruction of micelles.[14, 46-47] The classic pyrene-based fluorescent probe for the determination of CMC was thought to be non-ideal for the TD-FLV micelle system as the encapsulated probes would not accurately reflect the CMC of these telodendrimer micelles without disrupting the internal structure. Therefore we chose to use a non-invasive technique such as dynamic light scattering (DLS). To determine the CMC by DLS, the scattering intensity of the TD-FLV_n micelle solutions as a function of concentration was measured in addition to the hydrodynamic size (Figure 4). Figure 4b and 4c show the scattering intensities and autocorrelation functions obtained from TD-FLV8 micelle solutions of various concentrations from 0.001 to 100 μg/mL. At concentrations below 5 μg/mL, the scattering intensities were found to be similar to that of PBS buffer and fluctuated slightly around 200 kcps. The correlation functions obtained had very low intercepts less than 0.1, suggesting poor signal-to-noise ratios and no size-distribution information could be obtained, which was a clear indication these solutions contained mostly unimers. When the CMC was reached, the scattering intensity went up rapidly with increasing concentration due to the presence of large micelles formed. Using the intersection of the two slopes in Figure 4b, the CMC of TD-FLV8 micelle was calculated as 5 μg/mL (0.34 μM) in PBS buffer. The CMC of TD-FLV4, TD-FLV16 and fulvestrant-encapsulating (10 wt.% and 20 wt.%) TD-FLV8 micelles were determined following the same method and summarized in Figure S11 and Table 3. The low CMC values of these telodendrimer micelles indicate they are thermodynamically stable and show potential for drug delivery applications.

CMCs of the TD-FLV_n micelles were found to be highly dependent on the telodendrimer generation and the amount of drug encapsulated. Blank micelles prepared from TD-FLV4 had a CMC of 19 μg/mL (1.8 μM) and TD-FLV16 micelle has a CMC of 2 μg/mL (0.11 μM). This significant decrease in CMC can be attributed to and increasing the number of conjugated drugs. As the telodendrimer generation went up from 2 to 4, the number of fulvestrant attached at the dendritic block increased from 4 to 16 while the hydrophilic linear PSar remained the same length. Fulvestrant is a very hydrophobic molecule with a log P of 7.67 and contains an aromatic group and multiple hydrogen bond donors/acceptors. The dendritic architecture brings all the fulvestrant hydrophobes into close proximity and thus increasing the anchoring

effect which may also impact the observed reduction in CMC. Therefore the CMC decrease can be explained by the combination of the dendritic architecture with increasing hydrophobic interaction, π-π stacking[48] and hydrogen bonding[20] within the drug-conjugated block. Similarly, the same decreasing trend in CMC was also observed among the fulvestrant-encapsulating micelles, where low loading (10 wt.%) TD-FLV8 micelle showing a higher CMC (10 µg/mL) compared to high loading micelle (20 wt.%, 6 µg/mL).

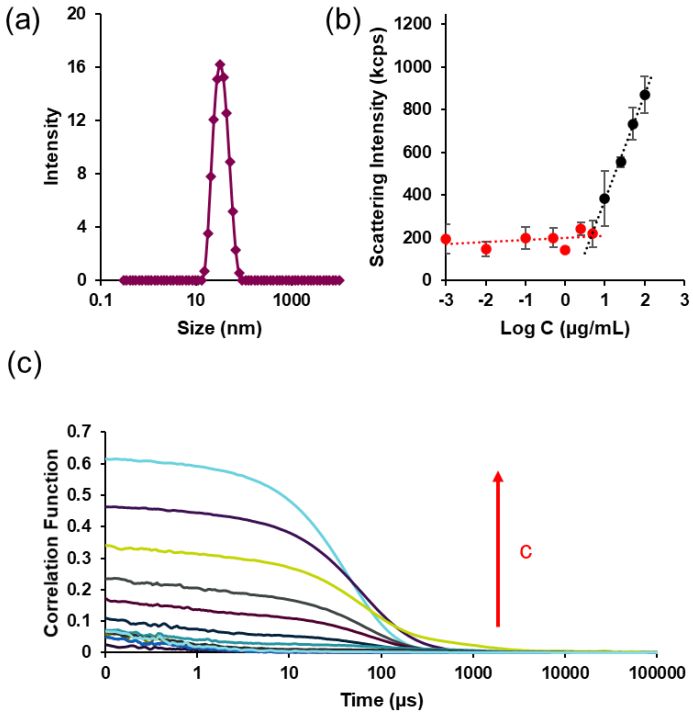

Figure 4. Characteristics of TD-FLV8 self-assembled micelles from DLS. (a) Intensity average size of 30 nm with PDI 0.069. Determination of CMC using (b) scattering intensity as a function of micelle mass concentration in PBS buffer. (c) Autocorrelation functions obtained at various micelle concentrations from 100 to 0.001 µg/mL (top to bottom).

Mass photometry for characterization of telodendrimer micelles.

Mass photometry (MP) is an optical microscopy technique based on interferometric scattering mass spectrometry (iSCAT) that measures the mass of single particles in solution. MP can detect samples with molecular weights ranging from 40 to 4,000 kDa with high mass accuracy (< 2% deviation between measured and sequence mass)[49] and has been used primarily for protein characterization to obtain information such as mass, stoichiometry and heterogeneity.[50-51] Previously, MP has been reported to characterize PSar star polymers and the masses obtained were in good agreement with MD-SEC and MALDI-TOF-MS.[32] Therefore, a similar approach was taken to measure the mass of the telodendrimer micelles and to estimate their aggregation numbers.

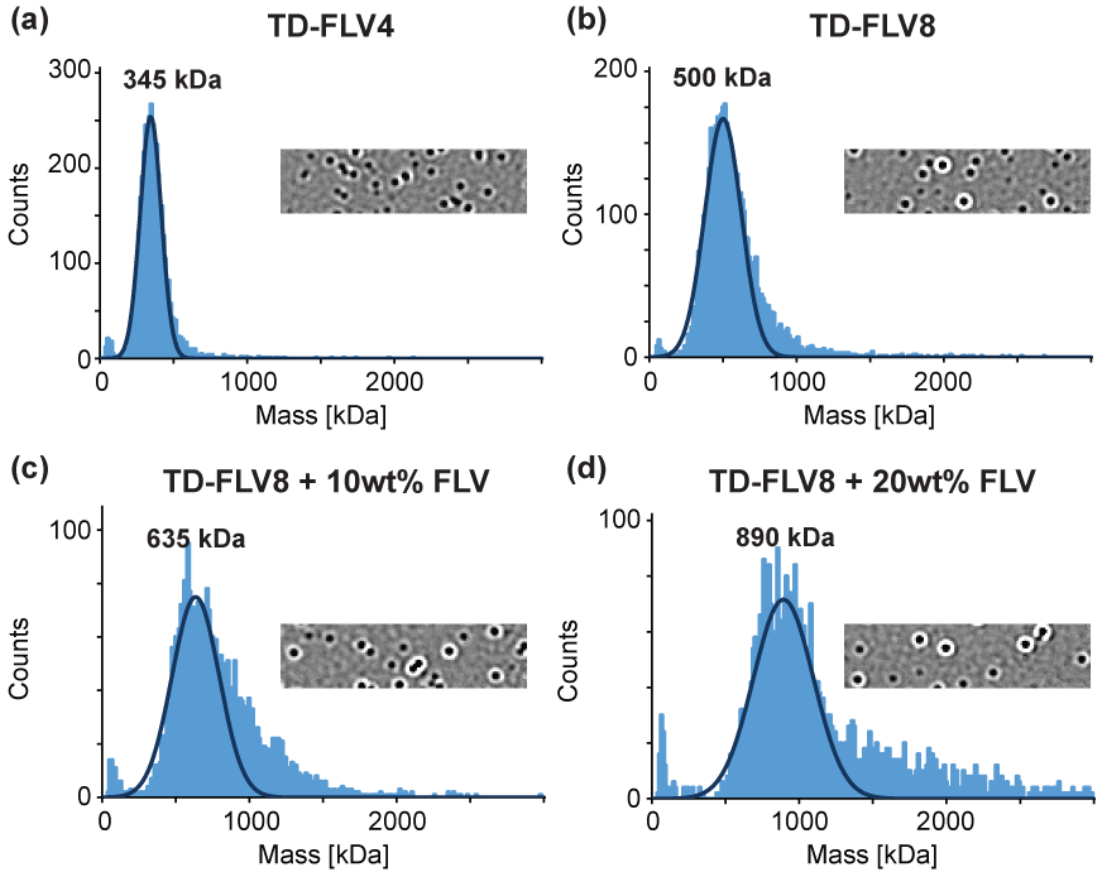

Figure 5. Mass photometry histograms showing (a) blank TD-FLV4 micelles, (b) blank TD-FLV8 micelles, (c) 10 wt.% and (d) 20 wt.% fulvestrant-encapsulating TD-FLV8 micelles with representative interferometric scattering images showing the contrasts.

Table 3. Characteristics of TD-FLV$_n$ micelles determined by DLS and Mass Photometry.

Samples	$MW_{telodendrimer}$	LC %	CMC[a] (μg/mL)	Molar $mass_{micelle}$[b]	N_{agg}	# of encapsulated drugs per micelle	total # of drugs per micelle
TD-FLV4[c]	10.3 kDa	-	18.6	345 kDa	34	0	140
TD-FLV8[c]	13.3 kDa	-	4.57	500 kDa	38	0	300
TD-FLV16[c]	20.3 kDa	-	2.14	NC	NC	NC	NC
TD-FLV8a[d]	-	12	9.55	635 kDa	43	110	450
TD-FLV8b[d]	-	23	5.75	890 kDa	54	300	730

[a] CMC determined from DLS. [b] Calculated micelle molar mass from mass photometry. NC - Not calculated – particle size beyond limit of MP instrumentation. [c] Blank micelles with no encapsulated drugs. [d] Drug-encapsulating micelles with 10 wt.% fulvestrant (size = 35 ± 0.4 nm, PDI = 0.14) and 20 wt.% fulvestrant (size = 40 ± 0.5 nm, PDI = 0.13), respectively.

Blank micelles of TD-FLV$_n$ (n = 4, 8, 16) and two fulvestrant-solubilizing (10 wt.% and 20 wt.%) TD-FLV8 micelles were examined by MP and the results obtained summarized in Table 3. Fitting the histograms with Gaussian fits, the average mass of the TD-FLV4 micelle was determined to be 345 kDa, from which we derive an aggregation number (N_{agg}) of 34 telodendrimer unimers. For TD-FLV8 micelle, a MW of 500 kDa with N_{agg} of 38 was obtained, which is in agreement with the increased micelle size determined from DLS. Two fulvestrant-encapsulating TD-FLV8 micelles were measured and analysed similarly. The representative interferometric scattering images in Figure 5 shows that the contrast of these four samples increased as micelle molecular weight increased. Unfortunately, TD-FLV16 micelle with a size of 116 nm was too large and beyond the MP working mass range, therefore we were unable to obtain any useful information. The high loading capacity of these telodendrimer micelles was reflected by the total number of drugs per micelle, where a single TD-FLV8 micelle could carry up to ~730 fulvestrant molecules.

Colloidal stability of telodendrimer micelles

The physical stability of TD-FLV8 telodendrimer micelles stored at 4°C in DI water with various amount of fulvestrant encapsulated was monitored by DLS over a period of one month (Figure S12). No significant increase in the size and PDI of the micelles was observed, indicating good colloidal stability and no micelle agglomeration.

***In vitro* release of fulvestrant from telodendrimer micelles.**

In our design, the fulvestrant was conjugated to the telodendrimers *via* an ester linker, providing a site for hydrolytic cleavage. To demonstrate drug could be released in a controlled manner, the hydrolysis of the TD-FLV8 micelle was monitored at 37 °C up to 1 week at pH 8.5, 7.4 and 5.5. The amount of drug released was quantified using UPLC. As shown in Figure 6, the release of fulvestrant from blank TD-FLV8 micelles after 24 h at pH 8.5, pH 7.4 and pH 5.5 was 52.8%, 21.2% and 1.3%, respectively. As expected for an ester linkage to the fulvestrant molecule, the bond was hydrolyzed very quickly at basic pH compared to neutral and pH 5.5 the latter where less than 10% drug was released after 168 h. The presence of protein can impact release rate by disrupting micelle structures.[52] To evaluate the effect of protein binding *in vitro*, the hydrolysis of TD-FLV8 micelles was also monitored at pH 7.4 in the presence of 45 mg/mL bovine serum albumin (BSA). Interestingly, the hydrolysis rate was very close to the one obtained in the absence of the protein, indicating the presence of BSA did not accelerate the release rate and suggesting protein binding did not interfere with the micellar structure owing to the stealth PSar corona and the high micelle stability.

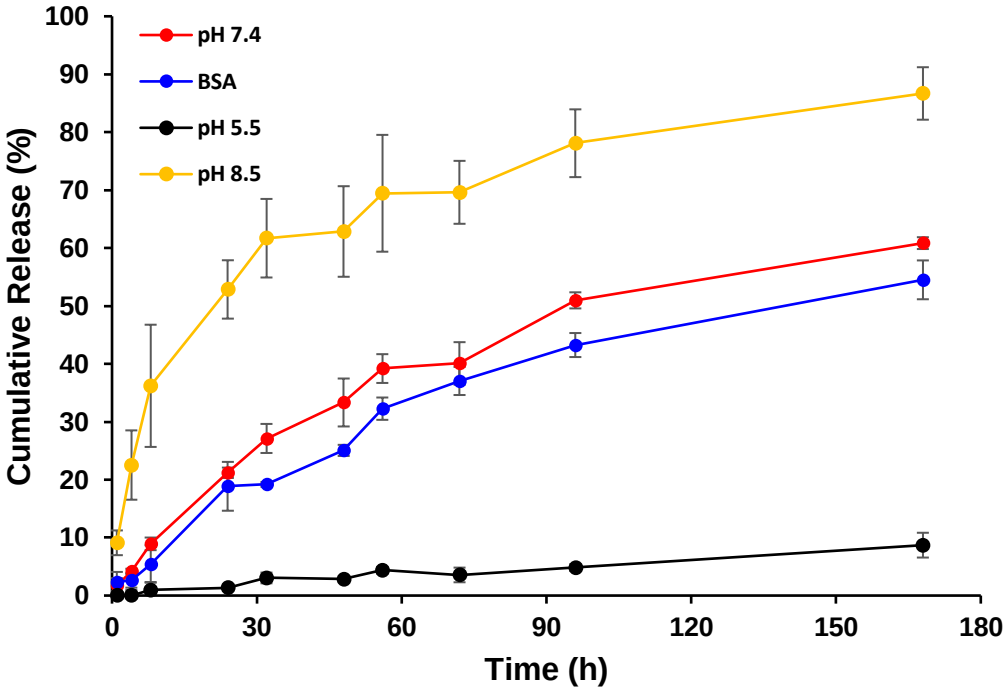

Figure 6. *In vitro* drug release profile of blank TD-FLV8 micelles at (a) pH 7.4, (b) pH 7.4 in presence of BSA, (c) pH 5.5, and (d) pH 8.5. All the experiments were conducted using three individually prepared samples and results are presented as mean ± standard deviation (SD).

Conclusion

In summary, we reported the synthesis of a poly(sarcosine)-*b*-poly(L-lysine) telodendrimer $PSar_{100}$-b-$PLL[FLV]_n^{Gm}$ in which *n* represents the number of fulvestrant molecules covalently attached at the periphery of the dendritic block, and G_m represents the lysine dendron generations 2-4. The telodendrimer was synthesized by polymerization of a linear PSar chain and divergent growth of a lysine dendron from the PSar chain terminal amine. The terminal amine groups of the lysine dendron were used to attach fulvestrant using a succinic acid linker. Self-assembly experiments showed all three telodendrimers TD-FLV4, TD-FLV8, and TD-FLV16 formed self-assemblies in water using a co-solvent evaporation method. The generation of telodendrimers and therefore the number of fulvestrant molecules on the dendritic block, strongly influenced the micelle physicochemical properties such as size, stability, and additional encapsulated drug loading capacity. A novel technique to the field, mass photometry was employed to estimate the number of unimers in the micelles and therefore the numbers of drug molecule/micelle in a facile way. From the different telodendrimers synthesized, the TD-FLV8 micelles exhibited the most tuneable sizes between 30-60 nm and high drug load of ~55 wt.% (combining conjugated and encapsulated drug), in combination

with excellent colloidal stability and high water solubility making them the most suitable candidate for the delivery of fulvestrant. We believe that the versatility of these telodendrimer-based micelle systems to both conjugate and encapsulate drug with high efficiency and stability, in addition to having other tuneable properties makes them a promising drug delivery system for a range of active pharmaceutical ingredients and therapeutic targets.

Reference

1. Peer, D.; Karp, J. M.; Hong, S.; Farokhzad, O. C.; Margalit, R.; Langer, R., Nanocarriers as an emerging platform for cancer therapy. *Nat Nanotechnol* **2007,** *2* (12), 751-760.
2. Matsumura, Y.; Kataoka, K., Preclinical and clinical studies of anticancer agent-incorporating polymer micelles. *Cancer Sci* **2009,** *100* (4), 572-579.
3. Ghosh, B.; Biswas, S., Polymeric micelles in cancer therapy: State of the art. *J Control Release* **2021,** *332*, 127-147.
4. Leroux, J. C., Editorial: Drug Delivery: Too Much Complexity, Not Enough Reproducibility? *Angew Chem Int Ed Engl* **2017,** *56* (48), 15170-15171.
5. Luxenhofer, R., Polymers and nanomedicine: considerations on variability and reproducibility when combining complex systems. *Nanomedicine (Lond)* **2015,** *10* (20), 3109-3119.
6. Kim, S.; Shi, Y.; Kim, J. Y.; Park, K.; Cheng, J. X., Overcoming the barriers in micellar drug delivery: loading efficiency, in vivo stability, and micelle-cell interaction. *Expert Opin Drug Deliv* **2010,** *7* (1), 49-62.
7. Zhang, Y.; Ren, T.; Gou, J.; Zhang, L.; Tao, X.; Tian, B.; Tian, P.; Yu, D.; Song, J.; Liu, X.; Chao, Y.; Xiao, W.; Tang, X., Strategies for improving the payload of small molecular drugs in polymeric micelles. *J Control Release* **2017,** *261*, 352-366.
8. Kaga, S.; Truong, N. P.; Esser, L.; Senyschyn, D.; Sanyal, A.; Sanyal, R.; Quinn, J. F.; Davis, T. P.; Kaminskas, L. M.; Whittaker, M. R., Influence of Size and Shape on the Biodistribution of Nanoparticles Prepared by Polymerization-Induced Self-Assembly. *Biomacromolecules* **2017,** *18* (12), 3963-3970.
9. Chithrani, B. D.; Ghazani, A. A.; Chan, W. C., Determining the size and shape dependence of gold nanoparticle uptake into mammalian cells. *Nano Lett* **2006,** *6* (4), 662-668.
10. Albanese, A.; Tang, P. S.; Chan, W. C., The effect of nanoparticle size, shape, and surface chemistry on biological systems. *Annu Rev Biomed Eng* **2012,** *14*, 1-16.
11. Venkataraman, S.; Hedrick, J. L.; Ong, Z. Y.; Yang, C.; Ee, P. L.; Hammond, P. T.; Yang, Y. Y., The effects of polymeric nanostructure shape on drug delivery. *Adv Drug Deliv Rev* **2011,** *63* (14-15), 1228-1246.
12. Wang, Z.; Deng, X.; Ding, J.; Zhou, W.; Zheng, X.; Tang, G., Mechanisms of drug release in pH-sensitive micelles for tumour targeted drug delivery system: A review. *Int J Pharm* **2018,** *535* (1-2), 253-260.
13. Ahmad, Z.; Shah, A.; Siddiq, M.; Kraatz, H.-B., Polymeric micelles as drug delivery vehicles. *RSC Adv.* **2014,** *4* (33), 17028-17038.
14. Owen, S. C.; Chan, D. P. Y.; Shoichet, M. S., Polymeric micelle stability. *Nano Today* **2012,** *7* (1), 53-65.
15. Kozlov, M. Y.; Melik-Nubarov, N. S.; Batrakova, E. V.; Kabanov, A. V., Relationship between Pluronic Block Copolymer Structure, Critical Micellization Concentration and Partitioning Coefficients of Low Molecular Mass Solutes. *Macromolecules* **2000,** *33* (9), 3305-3313.
16. Adams, M. L.; Kwon, G. S., Relative aggregation state and hemolytic activity of amphotericin B encapsulated by poly(ethylene oxide)-block–poly(N-hexyl-l-aspartamide)-acyl conjugate micelles: effects of acyl chain length. *Journal of Controlled Release* **2003,** *87* (1-3), 23-32.
17. Adams, M. L.; Kwon, G. S., The effects of acyl chain length on the micelle properties of poly(ethylene oxide)-block-poly(N-hexyl-L-aspartamide)-acyl conjugates. *J Biomater Sci Polym Ed* **2002,** *13* (9), 991-1006.

18. Van Domeselaar, G. H.; Kwon, G. S.; Andrew, L. C.; Wishart, D. S., Application of solid phase peptide synthesis to engineering PEO–peptide block copolymers for drug delivery. *Colloids and Surfaces B: Biointerfaces* **2003,** *30* (4), 323-334.
19. Cabral, H.; Kataoka, K., Progress of drug-loaded polymeric micelles into clinical studies. *J Control Release* **2014,** *190*, 465-476.
20. Kim, S. H.; Tan, J. P.; Nederberg, F.; Fukushima, K.; Colson, J.; Yang, C.; Nelson, A.; Yang, Y. Y.; Hedrick, J. L., Hydrogen bonding-enhanced micelle assemblies for drug delivery. *Biomaterials* **2010,** *31* (31), 8063-8071.
21. Lv, S.; Wu, Y.; Cai, K.; He, H.; Li, Y.; Lan, M.; Chen, X.; Cheng, J.; Yin, L., High Drug Loading and Sub-Quantitative Loading Efficiency of Polymeric Micelles Driven by Donor-Receptor Coordination Interactions. *J Am Chem Soc* **2018,** *140* (4), 1235-1238.
22. Aliabadi, H. M.; Lavasanifar, A., Polymeric micelles for drug delivery. *Expert Opin Drug Deliv* **2006,** *3* (1), 139-162.
23. Lübtow, M. M.; Hahn, L.; Haider, M. S.; Luxenhofer, R., Drug Specificity, Synergy and Antagonism in Ultrahigh Capacity Poly(2-oxazoline)/Poly(2-oxazine) based Formulations. *J Am Chem Soc* **2017,** *139* (32), 10980-10983.
24. Lübtow, M. M.; Haider, M. S.; Kirsch, M.; Klisch, S.; Luxenhofer, R., Like Dissolves Like? A Comprehensive Evaluation of Partial Solubility Parameters to Predict Polymer-Drug Compatibility in Ultrahigh Drug-Loaded Polymer Micelles. *Biomacromolecules* **2019,** *20* (8), 3041-3056.
25. He, Z.; Wan, X.; Schulz, A.; Bludau, H.; Dobrovolskaia, M. A.; Stern, S. T.; Montgomery, S. A.; Yuan, H.; Li, Z.; Alakhova, D.; Sokolsky, M.; Darr, D. B.; Perou, C. M.; Jordan, R.; Luxenhofer, R.; Kabanov, A. V., A high capacity polymeric micelle of paclitaxel: Implication of high dose drug therapy to safety and in vivo anti-cancer activity. *Biomaterials* **2016,** *101*, 296-309.
26. Lübtow, M. M.; Nelke, L. C.; Seifert, J.; Kuhnemundt, J.; Sahay, G.; Dandekar, G.; Nietzer, S. L.; Luxenhofer, R., Drug induced micellization into ultra-high capacity and stable curcumin nanoformulations: Physico-chemical characterization and evaluation in 2D and 3D in vitro models. *J Control Release* **2019,** *303*, 162-180.
27. Mikhail, A. S.; Allen, C., Poly(ethylene glycol)-b-poly(epsilon-caprolactone) micelles containing chemically conjugated and physically entrapped docetaxel: synthesis, characterization, and the influence of the drug on micelle morphology. *Biomacromolecules* **2010,** *11* (5), 1273-1280.
28. Shi, C.; Guo, D.; Xiao, K.; Wang, X.; Wang, L.; Luo, J., A drug-specific nanocarrier design for efficient anticancer therapy. *Nat Commun* **2015,** *6*, 1-14.
29. Huang, W.; Wang, X.; Shi, C.; Guo, D.; Xu, G.; Wang, L.; Bodman, A.; Luo, J., Fine-tuning vitamin E-containing telodendrimers for efficient delivery of gambogic acid in colon cancer treatment. *Mol Pharm* **2015,** *12* (4), 1216-1229.
30. Moquin, A.; Sturn, J.; Zhang, I.; Ji, J.; von Celsing, R.; Vali, H.; Maysinger, D.; Kakkar, A., Unraveling Aqueous Self-Assembly of Telodendrimers to Shed Light on Their Efficacy in Drug Encapsulation. *ACS Applied Bio Materials* **2019,** *2* (10), 4515-4526.
31. Raw, S. A., An improved process for the synthesis of DMTMM-based coupling reagents. *Tetrahedron Letters* **2009,** *50* (8), 946-948.
32. England, R. M.; Moss, J. I.; Gunnarsson, A.; Parker, J. S.; Ashford, M. B., Synthesis and Characterization of Dendrimer-Based Polysarcosine Star Polymers: Well-Defined, Versatile Platforms Designed for Drug-Delivery Applications. *Biomacromolecules* **2020,** *21* (8), 3332-3341.
33. Wurm, F.; Frey, H., Linear–dendritic block copolymers: The state of the art and exciting perspectives. *Progress in Polymer Science* **2011,** *36* (1), 1-52.

34. Xiao, K.; Luo, J.; Fowler, W. L.; Li, Y.; Lee, J. S.; Xing, L.; Cheng, R. H.; Wang, L.; Lam, K. S., A self-assembling nanoparticle for paclitaxel delivery in ovarian cancer. *Biomaterials* **2009,** *30* (30), 6006-6016.
35. Robertson, J. F.; Harrison, M., Fulvestrant: pharmacokinetics and pharmacology. *Br J Cancer* **2004,** *90 Suppl 1*, S7-10.
36. Weber, B.; Birke, A.; Fischer, K.; Schmidt, M.; Barz, M., Solution Properties of Polysarcosine: From Absolute and Relative Molar Mass Determinations to Complement Activation. *Macromolecules* **2018,** *51* (7), 2653-2661.
37. Birke, A.; Ling, J.; Barz, M., Polysarcosine-containing copolymers: Synthesis, characterization, self-assembly, and applications. *Progress in Polymer Science* **2018,** *81*, 163-208.
38. Son, K.; Ueda, M.; Taguchi, K.; Maruyama, T.; Takeoka, S.; Ito, Y., Evasion of the accelerated blood clearance phenomenon by polysarcosine coating of liposomes. *J Control Release* **2020,** *322*, 209-216.
39. Nogueira, S. S.; Schlegel, A.; Maxeiner, K.; Weber, B.; Barz, M.; Schroer, M. A.; Blanchet, C. E.; Svergun, D. I.; Ramishetti, S.; Peer, D.; Langguth, P.; Sahin, U.; Haas, H., Polysarcosine-Functionalized Lipid Nanoparticles for Therapeutic mRNA Delivery. *ACS Applied Nano Materials* **2020,** *3* (11), 10634-10645.
40. Cheng, L.; Cao, D., Effect of tail architecture on self-assembly of amphiphiles for polymeric micelles. *Langmuir* **2009,** *25* (5), 2749-2756.
41. Cheng, C.-C.; Sun, Y.-T.; Lee, A.-W.; Huang, S.-Y.; Fan, W.-L.; Chiao, Y.-H.; Chiu, C.-W.; Lai, J.-Y., Hydrogen-bonded supramolecular micelle-mediated drug delivery enhances the efficacy and safety of cancer chemotherapy. *Polymer Chemistry* **2020,** *11* (16), 2791-2798.
42. Luxenhofer, R.; Schulz, A.; Roques, C.; Li, S.; Bronich, T. K.; Batrakova, E. V.; Jordan, R.; Kabanov, A. V., Doubly amphiphilic poly(2-oxazoline)s as high-capacity delivery systems for hydrophobic drugs. *Biomaterials* **2010,** *31* (18), 4972-4979.
43. Haider, M. S.; Lübtow, M. M.; Endres, S.; Forster, S.; Flegler, V. J.; Bottcher, B.; Aseyev, V.; Poppler, A. C.; Luxenhofer, R., Think Beyond the Core: Impact of the Hydrophilic Corona on Drug Solubilization Using Polymer Micelles. *ACS Appl Mater Interfaces* **2020,** *12* (22), 24531-24543.
44. National Center for Biotechnology Information (2021). PubChem Compound Summary for CID 104741, Fulvestrant. . https://pubchem.ncbi.nlm.nih.gov/compound/Fulvestrant. (accessed May 24).
45. Shen, S.; Wu, Y.; Liu, Y.; Wu, D., High drug-loading nanomedicines: progress, current status, and prospects. *Int J Nanomedicine* **2017,** *12*, 4085-4109.
46. Shi, Y.; Lammers, T.; Storm, G.; Hennink, W. E., Physico-Chemical Strategies to Enhance Stability and Drug Retention of Polymeric Micelles for Tumor-Targeted Drug Delivery. *Macromol Biosci* **2017,** *17* (1), 1600160.
47. Lu, Y.; Zhang, E.; Yang, J.; Cao, Z., Strategies to improve micelle stability for drug delivery. *Nano Res* **2018,** *11* (10), 4985-4998.
48. Shi, Y.; van Steenbergen, M. J.; Teunissen, E. A.; Novo, L.; Gradmann, S.; Baldus, M.; van Nostrum, C. F.; Hennink, W. E., Pi-pi stacking increases the stability and loading capacity of thermosensitive polymeric micelles for chemotherapeutic drugs. *Biomacromolecules* **2013,** *14* (6), 1826-1837.
49. Young, G.; Hundt, N.; Cole, D.; Fineberg, A.; Andrecka, J.; Tyler, A.; Olerinyova, A.; Ansari, A.; Marklund, E. G.; Collier, M. P.; Chandler, S. A.; Tkachenko, O.; Allen, J.; Crispin, M.; Billington, N.; Takagi, Y.; Sellers, J. R.; Eichmann, C.; Selenko, P.; Frey, L.; Riek, R.; Galpin, M. R.; Struwe, W. B.; Benesch, J. L. P.; Kukura, P., Quantitative mass imaging of single biological macromolecules. *Science* **2018,** *360* (6387), 423-427.

50. Sonn-Segev, A.; Belacic, K.; Bodrug, T.; Young, G.; VanderLinden, R. T.; Schulman, B. A.; Schimpf, J.; Friedrich, T.; Dip, P. V.; Schwartz, T. U.; Bauer, B.; Peters, J. M.; Struwe, W. B.; Benesch, J. L. P.; Brown, N. G.; Haselbach, D.; Kukura, P., Quantifying the heterogeneity of macromolecular machines by mass photometry. *Nat Commun* **2020,** *11* (1), 1772-1781.
51. Olerinyova, A.; Sonn-Segev, A.; Gault, J.; Eichmann, C.; Schimpf, J.; Kopf, A. H.; Rudden, L. S. P.; Ashkinadze, D.; Bomba, R.; Frey, L.; Greenwald, J.; Degiacomi, M. T.; Steinhilper, R.; Killian, J. A.; Friedrich, T.; Riek, R.; Struwe, W. B.; Kukura, P., Mass Photometry of Membrane Proteins. *Chem* **2020**.
52. Lu, J.; Owen, S. C.; Shoichet, M. S., Stability of Self-Assembled Polymeric Micelles in Serum. *Macromolecules* **2011,** *44* (15), 6002-6008.